Research article

Sang Hyun Park[a], Sung-Gyu Lee[a], Soojeong Baek, Taewoo Ha, Sanghyub Lee, Bumki Min, Shuang Zhang, Mark Lawrence* and Teun-Teun Kim*

Observation of an exceptional point in a non-Hermitian metasurface

https://doi.org/10.1515/nanoph-2019-0489
Received November 29, 2019; revised January 19, 2020; accepted January 20, 2020

Abstract: Exceptional points (EPs), also known as non-Hermitian degeneracies, have been observed in parity-time symmetric metasurfaces as parity-time symmetry breaking points. However, the parity-time symmetry condition puts constraints on the metasurface parameter space, excluding the full examination of unique properties that stem from an EP. Here, we thus design a general non-Hermitian metasurface with a unit cell containing two orthogonally oriented split-ring resonators (SRRs) with overlapping resonance but different scattering rates and radiation efficiencies. Such a design grants us full access to the parameter space around the EP. The parameter space around the EP is first examined by varying the incident radiation frequency and coupling between SRRs. We further demonstrate that the EP is also observable by varying the incident radiation frequency along with the incident angle. Through both methods, we validate the existence of an EP by observing unique level crossing behavior, eigenstate swapping under encirclement, and asymmetric transmission of circularly polarized light.

Keywords: metamaterials; non-Hermitian photonics; exceptional point; asymmetric polarization conversion; phase singularity.

1 Introduction

When studying the physics of closed systems in which the conservation of energy is strictly obeyed, Hamiltonians are assumed to be Hermitian due to the many appropriate mathematical constraints it puts on the system, such as realness of eigenvalues, existence of an orthonormal basis, and unitary time evolution. Many systems in physics are, however, conveniently described by open systems, which may either gain or lose energy through interactions with its environment, resulting in complex eigenenergies. Such open systems are represented by non-Hermitian Hamiltonians.

One of the most interesting aspects of non-Hermitian (open) systems is their degeneracies, also known as exceptional points (EPs), in which both complex eigenvalues and eigenvectors of the system coalesce to form a defective eigenspace [1–4]. Unlike the Dirac point, which is unstable under perturbations in two dimensions, the EP is topologically robust, making it an ubiquitous feature among non-Hermitian systems. The significance of EPs has frequently been noted in non-Hermitian systems with special constraint of being parity-time symmetric. In these parity-time symmetric systems, the EP is shown to be the point of the parity-time symmetry breaking transition [5–12]. Beyond being the phase transition point of parity-time symmetric systems, EPs have unique properties due to the underlying geometry of their complex parameter spaces. Mathematically, the complex parameter space forms a self-intersecting Riemann sheet

[a]**Sang Hyun Park and Sung-Gyu Lee:** These authors contributed equally to this work.
***Corresponding authors: Mark Lawrence,** Department of Materials Science and Engineering, Stanford University, Stanford, CA 94305, USA, e-mail: markl89@stanford.edu; and **Teun-Teun Kim,** Center for Integrated Nanostructure Physics (CINAP), Institute for Basic Science (IBS), Suwon 16419, Republic of Korea; and Department of Physics, Sungkyunkwan University, Suwon 16419, Republic of Korea, e-mail: t.kim@skku.edu. https://orcid.org/0000-0002-4154-9775
Sang Hyun Park: Center for Integrated Nanostructure Physics (CINAP), Institute for Basic Science (IBS), Suwon 16419, Republic of Korea
Sung-Gyu Lee, Taewoo Ha and Sanghyub Lee: Center for Integrated Nanostructure Physics (CINAP), Institute for Basic Science (IBS), Suwon 16419, Republic of Korea; and Department of Energy Science, Sungkyunkwan University, Suwon 16419, Republic of Korea. https://orcid.org/0000-0003-3757-5863 (S.-G. Lee)
Soojeong Baek and Bumki Min: Department of Mechanical Engineering, Korea Advanced Institute of Science and Technology (KAIST), Daejeon 34141, Republic of Korea
Shuang Zhang: School of Physics and Astronomy, University of Birmingham, Birmingham B15 2TT, United Kingdom

in which the point of intersection is the EP. The nontrivial topology in the parameter space gives rise to intriguing phenomena, such as unconventional level crossing behavior [13, 14], increased sensitivity to perturbations [15–18], and observation of geometric phase under encirclement [19–23]. Such behavior has been observed using microwave cavities, chaotic optical cavities, and exciton-polariton billiards.

Metasurfaces, two-dimensional arrays of artificially designed subwavelength structures, provide an interesting platform for exploring the physics of EPs. The ability to tune the transmission needed to probe the parameter space in the vicinity of an EP is readily provided in metasurfaces by the variability of array parameters or input frequency. Moreover, measuring the transmission of the metasurface yields "complex" transmission eigenvalues, which is crucial to observing the properties of the EP and non-Hermitian matrices. Indeed, EPs have been observed as a phase transition point in parity-time symmetric metasurfaces [9, 10]. Although the constraints of parity-time symmetry provide a straightforward path for navigating directly through the EP, they also restrict us from exploring the full parameter space around the EP.

In this paper, we demonstrate that topologically robust EPs and phase singularities can be observed in a non-Hermitian metasurface. By designing a metasurface composed of hybrid meta-atoms with anisotropic radiation loss, the polarization eigenstates of the metasurface can be manipulated through variation of radiation frequency and meta-atom separation. By analyzing the transmission of the metasurface, we observe phenomena unique to EPs, including unconventional level crossing behavior, eigenstate swapping under encirclement of the EP, and asymmetric transmission of circularly polarized radiation. We have also observed a polarization phase singularity for the first time at an EP in the transmission through an anisotropic metasurface. The increased sensitivity to perturbations near the EP implies that the abrupt phase change observed at the singularity may be used in sensing applications [24–26]. Finally, we demonstrate that the EP can be observed without repeated fabrication of samples by simply altering the incident angle of radiation. This method provides a path to observing phenomena related to the dynamic encircling of the EP [27].

2 Results and discussion

2.1 Unit cell design

In this section, we discuss the design of the metasurface unit cell and how it gives a non-Hermitian transmission matrix. The metasurface is composed of an array with two orthogonally oriented split-ring resonators (SRRs) in each unit cell (Figure 1A). The two SRRs in a unit cell are modeled as an effective dipole moment $p_{x,y} = \tilde{p}_{x,y} e^{i\omega t}$, which couple strongly to an incident radiation field $E_i = \tilde{E}_i e^{i\omega t}$ with a radiative coupling strength g_i. The geometry and material of the SRR determine the resonance frequency, damping coefficient, and radiative coupling strength of the effective dipole moments. For incident radiation that is close to resonance ($\delta = \omega - \omega_0 \approx 0$) and assuming small damping ($\gamma \ll \omega_0$), the governing equation for the dipole moments is given by

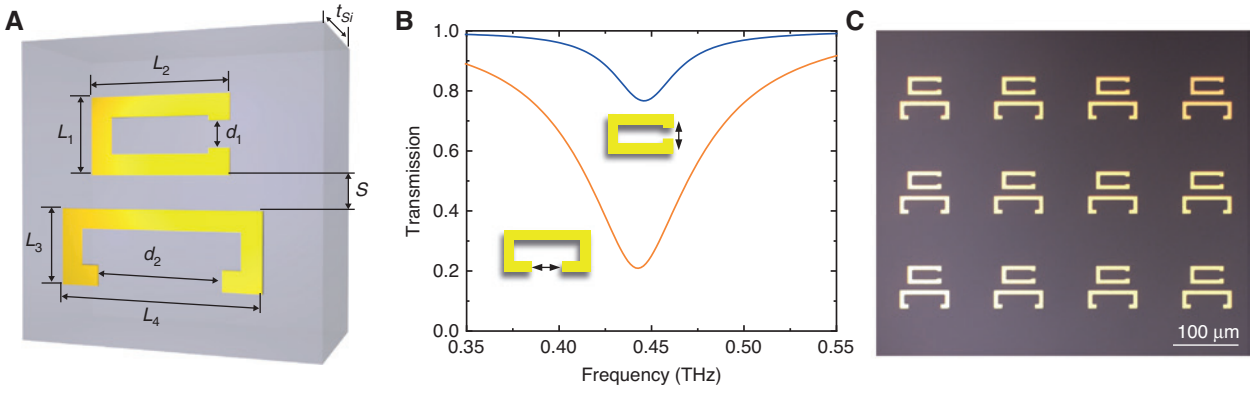

Figure 1: Structure of the non-Hermitian metasurface with the transmission spectrum of its resonator components.
(A) Schematic of the unit cell geometry. Dimensions are set to $L_1 = L_3 = 30$, $L_2 = 55$, $L_4 = 80$, $d_1 = 10$, $d_2 = 50$, $t_{Si} = 525$. All units are in μm. The dimensions of each SRR are optimized such that they have an equal resonance frequency while having different gap sizes. The difference in gap size makes the transmission matrix dispersive, thus letting us control the eigenstates of the system by changing the frequency of incident radiation. (B) Independent transmission plots for the orthogonally oriented SRRs in the unit cell. Each SRR was excited by incident radiation polarized parallel to the gap direction. (C) Top-view microscopic image of the fabricated metasurface.

$$\left[\begin{pmatrix}\delta_x+i\gamma_x & 0\\ 0 & \delta_y+i\gamma_y\end{pmatrix}+\begin{pmatrix}G_{xx} & G_{xy}\\ G_{yx} & G_{yy}\end{pmatrix}\right]\begin{pmatrix}p_x\\ p_y\end{pmatrix}=\begin{pmatrix}g_xE_{ix}\\ g_yE_{iy}\end{pmatrix}, \quad (1)$$

where G_{ij} is a summation of the i-oriented radiation fields formed by the j-oriented dipole moments. As the coupling terms G_{ij} depend only on the lattice geometry, the use of a square unit cell enforces the conditions $G_{xx}=G_{yy}$ and $G_{xy}=G_{yx}$. Furthermore, as the dipoles are orthogonally oriented and in the same plane, it follows that coupling between the dipoles only occurs via near-field quasi-static radiation, resulting in a real-valued G_{xy}. Although aligning the resonance frequencies of the SRRs is not a necessary condition for observing the EP, to maximize the coupling between the two components, the resonance frequencies are aligned (Figure 1B).

The transmitted field can then be found by superposing the incident field and the field radiated in the forward direction due to the oscillating dipoles, given by $\frac{i\omega\eta_0}{2a^2}(g_xp_x, g_yp_y)$, where $\eta_0=\sqrt{\mu_0/\varepsilon_0}$ is the free space impedance and a is the lattice constant. The transmission matrix is then

$$T=\begin{pmatrix}g_x^2(\delta+i\gamma_y+G_{xx}) & -g_xg_yG_{xy}\\ -g_xg_yG_{xy} & g_y^2(\delta+i\gamma_x+G_{xx})\end{pmatrix}, \quad (2)$$

up to a term proportional to the identity matrix that will have no effect on the eigenstates of the system. As the transmission matrix is non-Hermitian, we expect to observe non-Hermitian phenomena in the transmission eigenvalues and eigenstates. The eigenstates are Jones vectors that represent polarization states, and the corresponding eigenvalues will give the magnitude and phase with which the eigenstates are transmitted. Note that if $g_x=g_y=g$, Eq. (2) can be rewritten as

$$g^2\left[(\delta+i\bar{\gamma}+G_{xx})\begin{pmatrix}1 & 0\\ 0 & 1\end{pmatrix}+\begin{pmatrix}i\gamma & -G_{xy}\\ -G_{xy} & -i\gamma\end{pmatrix}\right] \quad (3)$$

where $\bar{\gamma}=(\gamma_1+\gamma_2)/2$, $\gamma=(\gamma_1-\gamma_2)/2$. As the identity matrix has no effect on the eigenstates, the matrix eigenstates become dispersionless, with the eigenvalues only linearly depending on the incident radiation frequency. Moreover, we notice that the second term in the brackets is a parity-time symmetric matrix, indicating that we will observe the parity-time symmetric phase transition in the eigenvalues and eigenvectors of T. Thus, it is important to ensure that $g_x\neq g_y$, which is achieved by making the gaps of two orthogonally oriented SRRs different.

2.2 Methods

The system is first studied numerically using the commercial finite-element method solver CST Microwave Studio. We check to find a geometry that gives resonant frequencies in the terahertz (THz) range. The unit cell geometry of the metasurface used in the simulations and in subsequent experiments is shown in Figure 1A, with the resonant frequency of each SRR shown in Figure 1B.

The fabrication procedure of metasurfaces is achieved by conventional photolithography. A positive photoresist [AZ-GXR-601 (14cp); AZ Electronic Materials] is spin coated onto a silicon substrate with resistivity of ~10 W cm. Au/Cr (100/5 nm) is then evaporated and patterned as orthogonally oriented SRR array structures via a lift-off process.

Transmission spectra of the metasurface are characterized by THz time-domain spectroscopy (THz-TDS). THz-TDS yields both the magnitude and phase of the transmission spectrum in a single measurement, giving us easy access to the complex transmission eigenvalues of the metasurface. The THz signal is emitted by a commercial photoconductive antenna (iPCA, BATOP). An electro-optic sampling method with a 1-mm-thick ZnTe crystal is used to detect the transmitted THz signals. After taking the Fourier transform of the time signal and normalizing against transmission through the bare silicon substrate, this measurement results in a complex transmission spectrum characterizing the sample. The full 2×2 transmission matrix is measured on the linear polarization basis. The polarization of the incident and transmitted fields are fixed using two wire-grid polarizers on each side of the metasurface. Transmission for circularly polarized states is related to the transmission of linearly polarized states by

$$\begin{aligned}T_{cir}&=\begin{pmatrix}T_{LL} & T_{LR}\\ T_{RL} & T_{RR}\end{pmatrix}\\ &=\frac{1}{2}\begin{pmatrix}(T_{xx}+T_{yy})+i(T_{xy}-T_{yx}) & (T_{xx}-T_{yy})-i(T_{xy}+T_{yx})\\ (T_{xx}-T_{yy})+i(T_{xy}+T_{yx}) & (T_{xx}+T_{yy})-i(T_{xy}-T_{yx})\end{pmatrix}\end{aligned} \quad (4)$$

where T_{ij} indicates a transmitted wave with polarization i and an incident wave with polarization j.

2.3 Results

2.3.1 Eigenvalue surface topology

Here, we validate the existence of an EP by examining the transmission eigenvalue surface. As mentioned previously, the eigenvalue surface of a non-Hermitian matrix

forms a self-intersecting Riemann sheet in which the EP is located at the point of intersection (see Figure 2A). This type of topology is unique to non-Hermitian systems and not observed in Hermitian systems. For Hermitian systems, the eigenvalue surface forms a double-cone structure with the degeneracy located at the conical intersection. Hence, observing the self-intersecting Riemann surface structure will provide strong evidence for the observation of an EP.

A non-Hermitian degeneracy has a codimension of 2, meaning that we need two parameters to capture the degeneracy [2]. Based on the ease and independence with which they can be controlled, parameters ω and G_{xy} are chosen. ω is directly controlled through incident radiation and G_{xy} is controlled by changing the distance between SRRs in the unit cell [9, 10]. Computing the eigenvalues and eigenvectors of the transmission matrix given in Eq. (2), we find that EPs exist at $(\omega^{EP}, G_{xy}^{EP}) = \left(\omega_0, \pm\frac{g_x^2\gamma_y - g_y^2\gamma_x}{2g_xg_y}\right)$. When calculating the position of the EP, we assume that G_{xx} is negligible. This is because the largest contribution to G_{xx} comes from dipoles in neighboring unit cells, whereas G_{xy} has contributions from within the unit cell. The eigenstate at each EP is $(1, \pm i)/\sqrt{2}$, which corresponds to left and right circularly polarized light. In this paper, we focus on the EP with left circularly polarized light as its singular eigenstate.

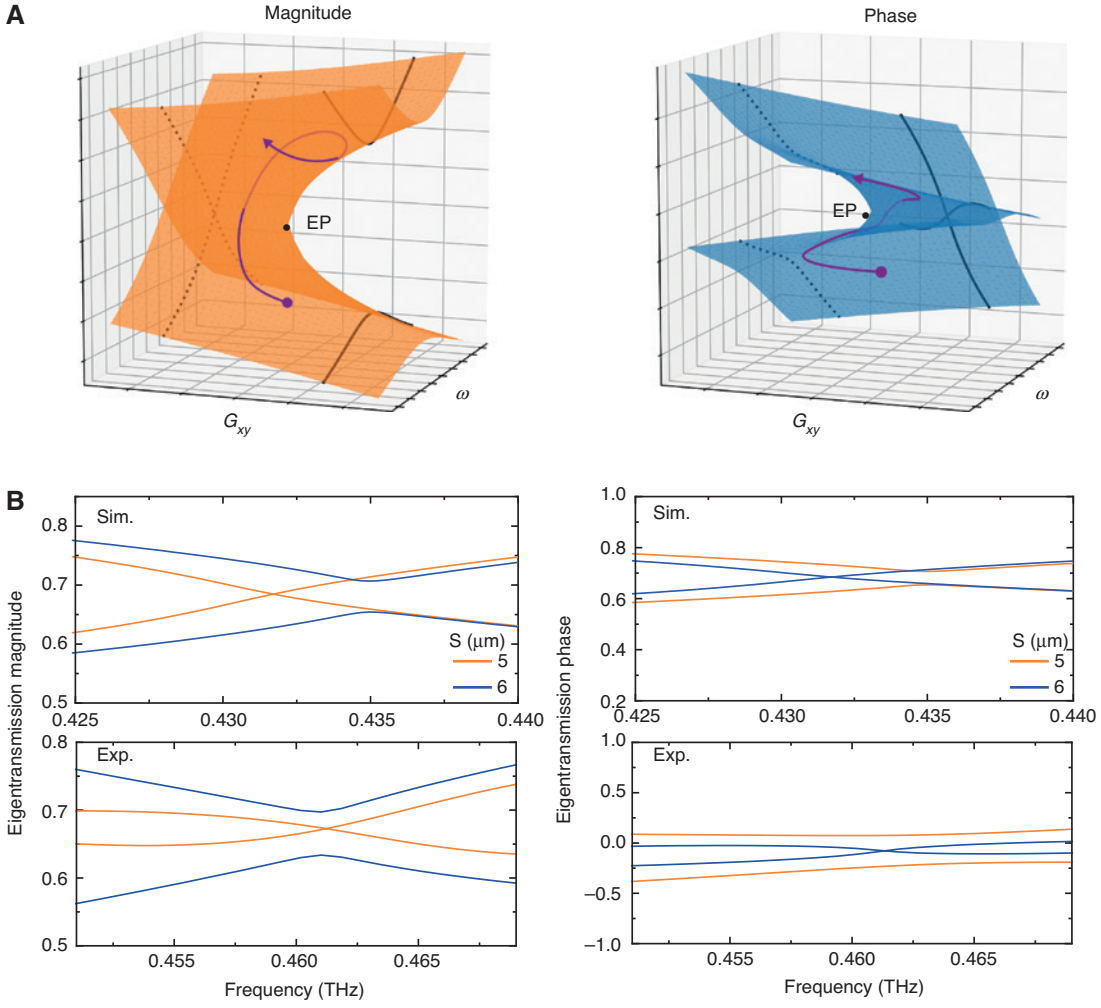

Figure 2: Eigenvalue surface topology near an exceptional point revealed through transmission simulation and experiment results of the non-Hermitian metasurface.
(A) Schematic of the complex eigenvalue surface in [ω, $G_{xy}(S)$] parameter space. At a given value of G_{xy}, we see that the crossing behavior as a function of frequency for the magnitude and phase of the eigenvalues is opposite. As the coupling is varied through the EP, the crossing behavior of the magnitude and phase are interchanged. Such behavior is a result of the unique topology of the self-intersecting Riemann surface formed in the vicinity of an EP. Purple lines show the evolution of the eigenvalues as the EP is encircled. (B) Simulation and experimental results of the complex eigenvalues as a function of frequency conducted at different separation S are shown. When $S = 5$ μm, we see that the magnitude the eigenvalues do not intersect while the phase crosses. When S is changed to 6 μm, the crossing behavior is swapped, and we see crossing in the magnitude and anti-crossing in the phase. As graphically shown in (A), this indicates that an EP exists between $S = 5$ μm and $S = 6$ μm.

The topology of the self-intersecting Riemann surface can be captured by observing the level crossing behavior in the magnitude and phase of the eigenvalues [13, 14]. Although it is usual to examine the real and imaginary parts of the eigenvalues, these quantities lack a direct physical interpretation for the complex transmission

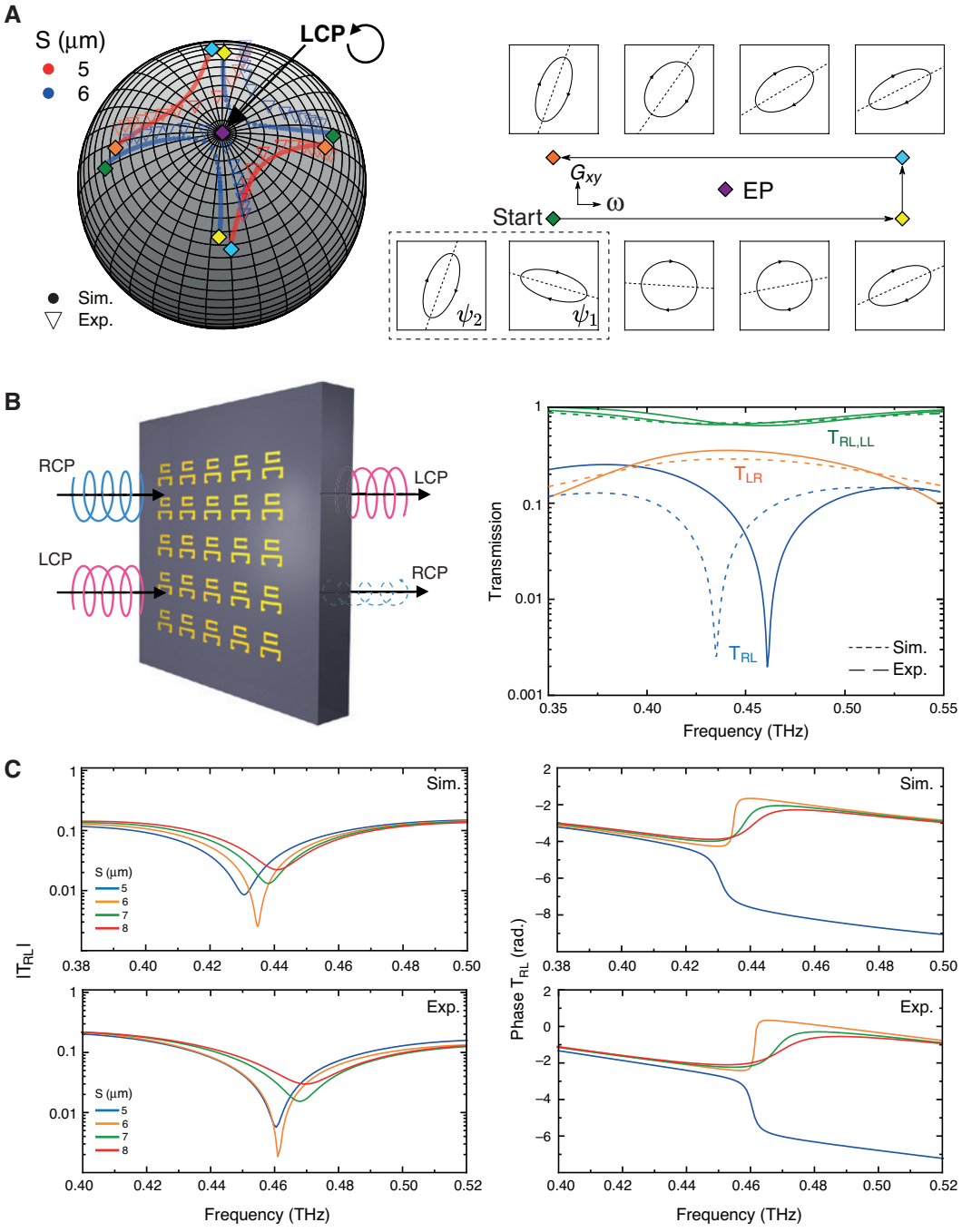

Figure 3: Eigenstate swapping and transmission phase singularity observed by changing coupling between resonator components. (A) Transmission eigenstates of the metasurface are plotted on a Poincaré sphere as the EP is encircled in the [ω, $G_{xy}(S)$] parameter space. Under one full loop around the EP, the states move halfway around the north pole of the Poincaré sphere, resulting in a swapping of eigenstates [i.e. $(\psi_1,\psi_2) \rightarrow (\psi_2,-\psi_1)$]. To the right of the Poincaré sphere, we explicitly show the evolution of polarization states. The states in the dashed box show the two eigenstates at the beginning of the loop. Thereafter, we follow how state ψ_1 evolves and find that it becomes ψ_2 at the end of a single loop. (B) The transmission matrix components in the circularly polarized basis are shown when $S=6$ μm. As we have anticipated from Eq. (5), T_{RR} and T_{LL} are identical, whereas T_{RL} is suppressed with respect to T_{LR}. The asymmetric transmission of circularly polarized light is a direct consequence of having a single eigenstate at the EP. (C) An abrupt phase flip in T_{RL} is observed as the parameter S is modulated through the EP.

eigenvalues. Therefore, we instead examine the magnitude and phase of the eigenvalues. As using the magnitude and phase instead of the real and imaginary parts of the eigenvalues can be considered as a mapping from Cartesian to polar coordinates in the complex plane, the topology near EPs will be preserved. When the value of G_{xy} is smaller than G_{xy}^{EP}, the magnitude (phase) of the eigenvalues anti-cross (cross). As G_{xy} is increased and passes through the EP, the crossing behavior interchanges such that the magnitude (phase) now cross (anti-cross). This type of crossing behavior is unique to non-Hermitian systems and cannot be observed in the double-cone eigenvalue surface of Hermitian systems.

The transmission eigenvalues calculated from simulation and experimental results are shown in Figure 2B. Assuming that the SRR separation distance S is inversely proportional to the coupling strength G_{xy}, we observe that the magnitude (phase) of the transmission eigenvalues change from anti-crossing (crossing) to crossing (anti-crossing) as coupling strength is increased. Such behavior exactly follows the topology of the self-intersecting Riemann surface and provides strong evidence that an EP is located in the parameter range $5 < S^{EP} < 6$.

2.3.2 Eigenstate swapping

The eigenvalue surface structure shown schematically in Figure 2A also reveals that the EP is a square-root branch point for the complex eigenvalues. This implies that the eigenvalues of the system will not return to their original values under one full loop around the EP but will rather be swapped. They will return to their original values only under two full loops. For the eigenstates, the EP is in fact a fourth-root branch point, meaning that four full loops are required to return the eigenstates to their initial states [2]. A single loop around the EP will interchange the two eigenstates and additionally accumulate a geometric phase of π on one of the states.

To show the swapping of eigenstates under encirclement, we follow the evolution of the transmission eigenstates by observing closely spaced stationary eigenstates of the metasurface. The eigenstates of the transmission matrix in Eq. (2) are polarization states that can be represented as polarization ellipses with ellipticity angle χ and orientation angle ψ. Polarization states are plotted on a Poincaré sphere for easy visualization.

Simulation and experimental data in Figure 3A show how the polarization eigenstates of the metasurface evolve as the parameters [ω, $G_{xy}(S)$] are encircled around the EP. On the Poincaré sphere, we plot the eigenstates of the system found from simulations for SRR separations 5 and 6 μm and frequency range 0.42–0.44 THz. Each parameter gives two eigenstates located on opposite sides of the sphere with respect to the north pole. Following the states along the parameter loop (ω, S) → (0.42, 5) → (0.44, 5) → (0.44, 6) → (0.42, 6) → (0.42, 5), we find that each state moves halfway around the north pole, resulting in a swapping of eigenstates. The polarization ellipses for the eigenstates along the encircling path are explicitly shown. States from experimental data are also plotted for SRR separations 5 and 6 μm and for a frequency range 0.45–0.47 THz. We find that the states from experimental data also result in a swapping of eigenstates under encircling of the EP. Although we should be able to observe an accumulation of geometric phases on one of the states, for our current setup, it cannot be measured. This is because measurements for different coupling values are conducted separately, thus making the phase relation between measurements ill-defined.

2.3.3 Asymmetric transmission of circularly polarized light

Due to the existence of a single transmission eigenstate at the EP, we expect that transmission should be asymmetric for right-handed circularly polarized (RCP) and left-handed circularly polarized (LCP) states when near the EP, which are associated with an abrupt change in phase. In general, the eigenstates of the system are given by $|\psi_1\rangle = \alpha|\mathrm{L}\rangle + \beta|R\rangle$ and $|\psi_2\rangle = \alpha|\mathrm{L}\rangle - \beta|R\rangle$. When the system is near the EP, both eigenstates are close to the $|L\rangle$ state. Therefore, we can assume that $|\alpha| \gg |\beta|$. As $T|\psi_i\rangle = \lambda_i|\psi_i\rangle$, we find the transmission behavior for the RCP and LCP states to be

$$T|L\rangle = \frac{\lambda_1+\lambda_2}{2}|L\rangle + \frac{\beta}{2\alpha}(\lambda_1-\lambda_2)|R\rangle \tag{5a}$$

$$T|R\rangle = \frac{\alpha}{2\beta}(\lambda_1-\lambda_2)|L\rangle + \frac{\lambda_1+\lambda_2}{2}|R\rangle. \tag{5b}$$

From Eqs. (5a) and (5b), we can expect that the direct transmission of RCP and LCP are identical. However, for cross-polarization conversion, the conversion from RCP to LCP is larger than the conversion from LCP to RCP by a factor of $(\alpha/\beta)^2$. As we have $|\alpha| \gg |\beta|$ near the EP, we expect to see an asymmetry in the transmission components T_{RL} and T_{LR} as the EP is approached.

We verify these predictions through simulation and experimental results for the transmission spectrum of the

metasurface. Figure 3B shows that the conversion from LCP to RCP (T_{RL}) is significantly lower than the conversion from RCP to LCP (T_{LR}) when the system is near the EP ($S=6$ μm). Physically, this can be understood from the fact that, near the EP, the amplitude of the RCP state is much smaller than the amplitude of the LCP state. Hence, it is relatively improbable for conversion from a high amplitude state to a low amplitude state to occur compared to conversion in the opposite direction. As the LCP state dominates more as the system approaches the EP, we expect the transmission asymmetry to also get larger. We notice that there is a mismatch of about 0.03 THz in the resonance peak between the simulation and experimental data. This discrepancy most likely stems from a difference in the refractive index of the silicon wafer substrate. Although we do not dismiss the discrepancy as trivial, we would like to point out that it is not a major issue in observing an EP. The shift in resonance frequency will simply result in the EP also being shifted in the parameter space. One can see that as the system approaches the EP, T_{RL} reaches almost zero and an abrupt jump in the phase of T_{RL} is observed despite a small change of coupling strength between two SRRs (Figure 3C). The sensitivity in phase dispersion for T_{RL} originates from the sensitivity of eigenvalues and eigenstates near the EP [15–18]. From Eq. (5), we find that the phase of T_{RL} depends on β/α and $\lambda_1 - \lambda_2$. As β/α gives the eigenstate position on the Poincaré sphere and $\lambda_1 - \lambda_2$ is the eigenvalue splitting, we see that sensitivity of the eigenvalues and eigenstates

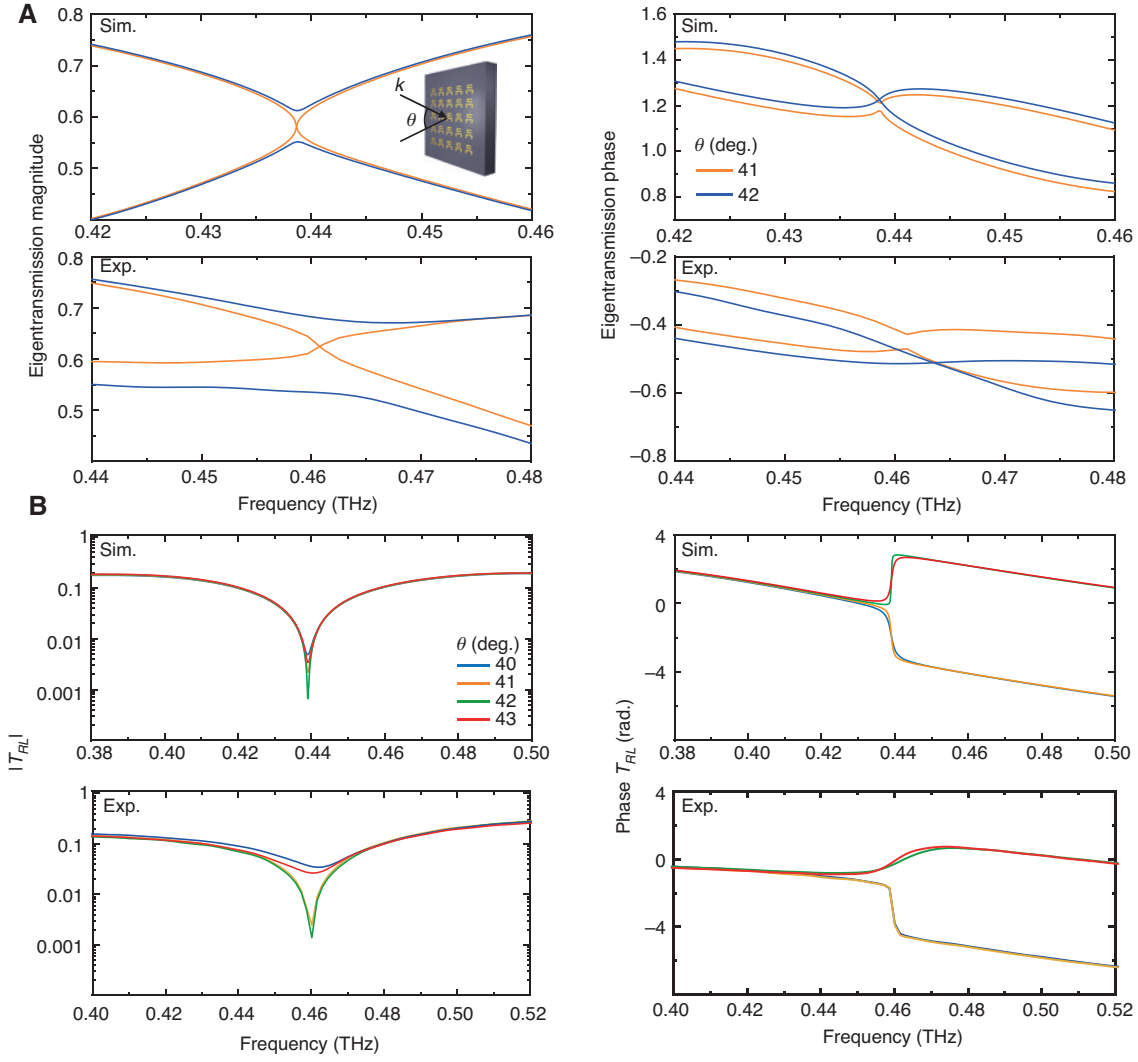

Figure 4: Eigenvalue surface topology and transmission phase singularity demonstrated by varying the incident angle of radiation. (A) The topology of the self-intersecting Riemann surface is observed in the [ω, $g_y(\theta)$] parameter space. Just as we have observed by varying G_{xy}, we see that the crossing behavior of the eigenvalue magnitude and phase are interchanged as g_y passes through the EP. From simulation and experimental results, we find that the EP located between $\theta=41°$ and 42°. (B) We observe an abrupt phase flip in T_{RL} as θ is varied through the EP.

directly translate into sensitivity of the T_{RL} phase. This rapid phase dispersion can be used for extremely sensitive biochemical detection [24–26].

2.3.4 Modulation of the incident angle of radiation

Up to this point, we have shown that an EP can be observed in our metasurface design through variation of the incident radiation frequency and separation between SRRs. Although this provides a straightforward and intuitive path to observing the EP, having to repeatedly fabricate new samples to change the SRR separation is a definite drawback. Repeated fabrication will inadvertently add fabrication errors, making it difficult to fine-tune parameters. When parameters are near the EP, errors are further amplified because the eigenvalues exhibit an enhanced sensitivity to perturbations [15, 16]. Moreover, we are also unable to perform dynamic encircling of the EP, which gives rise to phenomena such as time-asymmetric loops around the EP [27].

To overcome these limitations, we modulate the parameter g_y instead of G_{xy} by controlling the angle of incident radiation. By increasing the incident angle, we leave the in-plane x-component of the field unchanged while weakening the in-plane y-component and hence decreasing g_y. Using this method, we are capable of probing the parameter space with a single metasurface sample, freeing us from the limitations pointed out above.

We now show that the EP is observable in the $[\omega, g_y(\theta)]$ parameter space. In Figure 4A, the simulation and experimental data for the complex eigenvalues are shown. Just as we have seen by modulating the coupling strength, the magnitude (phase) of the eigenvalues change from crossing (anti-crossing) to anti-crossing (crossing) as the incident angle is modulated through the EP. This implies that the self-intersecting Riemann surface topology is also captured in the $[\omega, g_y(\theta)]$ parameter space. Figure 4B shows the magnitude and phase of the T_{RL} transmission matrix component. Once again, as expected from the properties of an EP, we see that the magnitude of T_{RL} decreases as the EP is approached accompanied with an abrupt phase jump.

3 Conclusion

In this work, we have designed a non-Hermitian metasurface composed of orthogonally oriented SRRs to observe an EP. By first controlling the radiation frequency and coupling between SRR elements, we have observed phenomena stemming from an EP, such as unique level crossing behavior, swapping of eigenstates under encirclement of the EP, asymmetric transmission of circularly polarized light, and an abrupt phase flip in the cross-polarization transmission. This abrupt phase change for circularly polarized light could have applications in devices, including active polarization modulator and sensitive biosensors. Our work also highlights that the EP can be observed without repeated fabrication of the metasurface by simply varying the incident angle of radiation, making it possible to observe phenomena related to dynamically encircling the EP. It would help to precisely locate the optimized operation point even after sample fabrication. By showing that an EP is observable in the polarization space of light, we open up a new platform for not only studying non-Hermitian physics but also developing very sensitive THz systems with nontrivial phase response.

Acknowledgments: This work was supported by the Institute for Basic Science of Korea (grant IBS-R011-D1, Funder Id: http://dx.doi.org/10.13039/501100010446), the National Research Foundation of Korea (NRF) through the Government of Korea (MSIP; grants NRF-2017R1A2B3012364, Funder Id: http://dx.doi.org/10.13039/501100003621, 2017M3C1A3013923, and 2015R1A5A6001948), and the Center for Advanced Meta-Materials funded by the Government of Korea (MSIP) as a Global Frontier Project (grant NRF-2014M3A6B3063709).

References

[1] Moiseyev N. Non-hermitian quantum mechanics, 1st ed. Cambridge, UK: Cambridge University Press, 2011.
[2] Heiss WD. Exceptional points of non-Hermitian operators. J Phys A Math Gen 2004;37:2455–64.
[3] Berry MV. Physics of nonhermitian degeneracies. Czechoslov J Phys 2004;54:1039–47.
[4] Miri MA, Alù A. Exceptional points in optics and photonics. Science 2019;363:eaar7709.
[5] Feng L, El-Ganainy R, Ge L. Non-Hermitian photonics based on parity-time symmetry. Nat Photonics 2017;11:752–62.
[6] El-Ganainy R, Makris KG, Khajavikhan M, Musslimani ZH, Rotter S, Christodoulides DN. Non-Hermitian physics and PT symmetry. Nat Phys 2018;14:11–9.
[7] Peng B, Ozdemir SK, Rotter S, et al. Loss-induced suppression and revival of lasing. Science 2014;346:328–32.
[8] Guo A, Salamo GJ, Duchesne D, et al. Observation of PT-symmetry breaking in complex optical potentials. Phys Rev Lett 2009;103:1–4.
[9] Bittner S, Dietz B, Günther U, et al. PT symmetry and spontaneous symmetry breaking in a microwave billiard. Phys Rev Lett 2012;108:1–5.

[10] Lawrence M, Xu N, Zhang X, et al. Manifestation of PT symmetry breaking in polarization space with terahertz metasurfaces. Phys Rev Lett 2014;113:1–5.
[11] Wang S, Wu PC, Su VC, et al. Broadband achromatic optical metasurface devices. Nat Commun 2017;8:1–9.
[12] Sakhdari M, Estakhri NM, Bagci H, Chen PY. Low-threshold lasing and coherent perfect absorption in generalized PT-symmetric optical structures. Phys Rev Appl 2018;10:1.
[13] Heiss WD, Sannino AL. Avoided level crossing and exceptional points. J Phys A Math Gen 1990;23:1167–78.
[14] Heiss WD. Repulsion of resonance states and exceptional points. Phys Rev E 1999;61:929–32.
[15] Wiersig J. Sensors operating at exceptional points: general theory. Phys Rev A 2016;93:1–9.
[16] Chen W, Ozdemir SK, Zhao G, Wiersig J, Yang L. Exceptional points enhance sensing in an optical microcavity. Nature 2017;548:192–5.
[17] Hodaei H, Hassan AU, Wittek S, et al. Enhanced sensitivity at higher-order exceptional points. Nature 2017;548:187–91.
[18] Chen PY, Sakhdari M, Hajizadegan M, et al. Generalized parity-time symmetry condition for enhanced sensor telemetry. Nat Electron 2018;1:297–304.
[19] Heiss WD. The physics of exceptional points. J Phys A Math Theor 2012;45:444016.
[20] Dembowski C, Dietz B, Graf HD, et al. Encircling an exceptional point. Phys Rev E 2004;69:056216.
[21] Dembowski C, Graf HD, Harney HL, et al. Experimental observation of the topological structure of exceptional points. Phys Rev Lett 2001;86:787–90.
[22] Gao T, Estrecho E, Bliokh KY, et al. Observation of non-Hermitian degeneracies in a chaotic exciton-polariton billiard. Nature 2015;526:554–8.
[23] Lee SB, Yang J, Moon S, et al. Observation of an exceptional point in a chaotic optical microcavity. Phys Rev Lett 2009;103:1–4.
[24] Kravets VG, Schedin F, Jalil R, et al. Singular phase nano-optics in plasmonic metamaterials for label-free single-molecule detection. Nat Mater 2013;12:304–9.
[25] Sreekanth KV, Sreejith S, Han S, et al. Biosensing with the singular phase of an ultrathin metal-dielectric nanophotonic cavity. Nat Commun 2018;9:369.
[26] Yesilkoy F, Terborg RA, Pello J, et al. Phase-sensitive plasmonic biosensor using a portable and large field-of-view interferometric microarray imager. Light Sci Appl 2018;7:17152.
[27] Yoon JW, Choi Y, Hahn C, et al. Time-asymmetric loop around an exceptional point over the full optical communications band. Nature 2018;562:86–90.